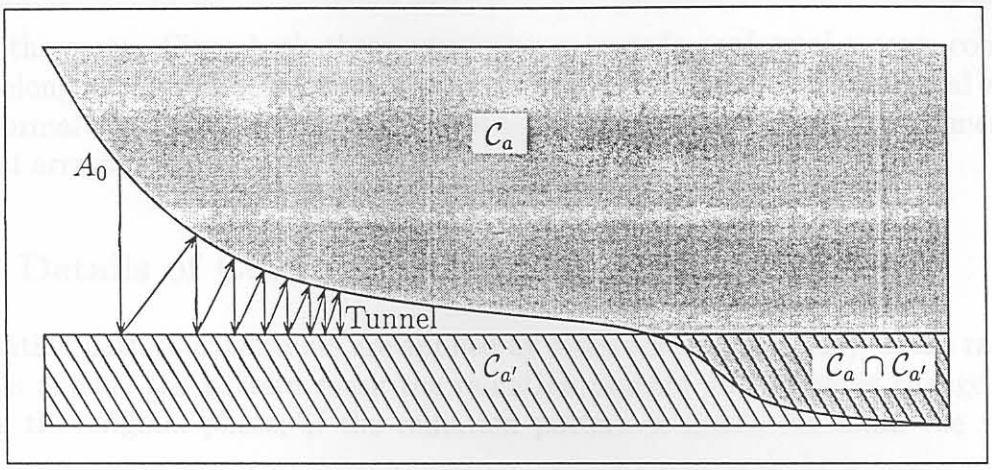

Figure 5.3: Illustrating tunnels, starting from $\vec{A}_0$ the sequence $\{\vec{A}_k\}$ converges to the true solution belonging to $C_a \cap C_{a'}$ through a long tunnel.

The effect of a tunnel is illustrated in Fig. 5.3. Relaxation, discussed in the previous section, can be used to alleviate this problem.

As stated earlier, a proper selection of the starting point is of the utmost importance, as a good starting point will be close enough to the final solution to avoid falling into a trap. Selecting a good starting point is not simple, the selection should take into account all the constraints. Various methods have been investigated, as discussed in Section 5.5.

5.4 Implementation Detail

In this section the computer program implementation of the intersection of sets synthesis technique will be discussed in some detail. However, before we embark on this discussion we need to define some terms.

Arrays with an array pattern of only one angular variable (say ϕ) will be referred to as one dimensional pattern arrays, or simply "one dimensional arrays". This class of arrays includes all linear arrays as well as conformal arrays where we are only interested in the pattern in the plane of the array.

Two dimensional pattern arrays, or simply "two dimensional arrays", are arrays with radiation patterns with two angular variables, (θ, ϕ). This class of arrays will include planar arrays where we are interested in a pattern in half-space; and conformal arrays where the radiation patterns are functions of both (θ, ϕ).

Although some arrays may seem to be a two dimensional array at first glance due to the array geometry, one has to consider the radiation pattern in order to classify the array. If the radiation pattern is of interest only in one plane, or dependent on only one angular variable, the array should be classified as a one dimensional array. An example of such an one dimensional array is an circular array which is used to scan 360° in the

plane of the array. Since both these array classes include conformal arrays, conformal arrays belonging to the first group will be called "one dimensional conformal arrays" and conformal arrays in the two dimensional array group will be called "two dimensional conformal arrays".

5.4.1 Details of Constraints on Radiation Pattern

The radiation pattern constraints are applied by means of a mask (5.44). If the radiation pattern is outside the pattern mask the radiation pattern magnitude is changed while retaining the original phase; if the radiation pattern is inside the mask the value is retained.

In the case of one dimensional arrays pencil beams as well as shaped beams can be synthesised. For shaped beams, the radiation pattern mask is described by a polynomial of the pattern angle $S(\theta)$ in the main or shaped beam region. This is often referred to as the shaping function. A zero to maximum ripple R specifies the acceptable level above and below the shaping function. The pattern mask in the shaped beam region is

$$S_U(\theta) = S(\theta) + R \quad \text{and} \quad S_L(\theta) = S(\theta) - R. \tag{5.69}$$

To set the main beam peak at 0dB the absolute level of the shaping function must be allowed to move up or down slightly. Since the shaping function is in polynomial form, the constant term can be used to control the shaping function level. On each side of the main beam, between the main beam region and the sidelobe regions is a transition region. The width of the transition regions control the roll-off from the main beam to the sidelobe level.

In the case of two dimensional arrays shaped beam patterns as well as contoured footprint patterns can be synthesised. Contoured patterns are described by a set of θ-values for a number of ϕ-cuts; the first θ-value indicates the end of the main beam region and the second indicates the start of the sidelobe region. The ripple inside the main beam must also be specified.

Shaped beams are specified in one ϕ in the same manner as for the one dimensional arrays. Similar to the contoured beam specification, θ-values in a number of ϕ-cuts are used to control the main beam roll-off. The software is written such that the shaped beam can only be specified in the $\phi = 0°$ -cut and the direction $(0, 0)$ must be in the main beam region.

The side lobe region, for all the different pattern types have a default sidelobe level. In addition to the default sidelobe level the sidelobe region can by divided into a number of piece wise linear subsections. Fixed nulls can also be specified anywhere in the sidelobe region, with a target suppression at each nulls.

In pattern synthesis we are interested in the radiated power, expressed in decibels. Thus both the pattern and the mask is in decibels. The error distance of the m-th pattern point of the k-th iteration is the distance between the pattern of the k-th iteration before

and after the application of the pattern mask:

$$\xi_{km} = 10\left|\log(|f'_m|^2) - \log(|f_m|^2)\right| \tag{5.70}$$

The total radiation pattern error at the k-th iteration is the average of the error distances at all pattern angles

$$\xi_k = \frac{1}{M}\sum_{m=1}^{M}\xi_{km} = \frac{10}{M}\sum_{m=1}^{M}\left|\log(|f'_m|^2) - \log(|f_m|^2)\right|. \tag{5.71}$$

If the weighted least squares inverse is used in the back projector relative weights must be assigned for each row of the radiation matrix. Aside from the default weight of one, the main lobe region and each sidelobe subregion are assigned a nominal weight according to its particular importance. Each of the fixed nulls are also assigned an individual weight. The relative weight of each pattern point is dependent on the error distance of that pattern point. The weight function consists of three linear sections:

$$w_m = w_0\begin{cases}1 & \text{if } \xi_{km} \le \xi_0\\ w_{slope}(\xi_{km} - \xi_0) & \text{if } \xi_0 \le \xi_{km} \le \xi_p\\ w_{peak} & \text{if } \xi_{km} \ge \xi_p\end{cases} \tag{5.72}$$

where ξ_0, w_{slope} and w_{peak} are specified by the user, w_0 is the default or nominal weight of the particular region and ξ_p is calculated from

$$\xi_p = \xi_0 + (w_{peak} - 1)/w_{slope}. \tag{5.73}$$

5.4.2 Detail of Constraints on Excitation

Four different excitation constraints have been implemented: symmetric, pure real and dynamic range and smoothness.

The excitation can be constrainted to be symmetric in both magnitude and phase

$$a_n = a_{N+1-n} = \tfrac{1}{2}(a'_n + a'_{N+1-n}) \tag{5.74}$$

or symmetry in just the magnitude only

$$\begin{aligned}|a_n| = |a_{N+1-n}| &= \tfrac{1}{2}\left(|a'_n| + |a'_{N+1-n}|\right)\\ \angle a_n &= \angle a'_n\\ \angle a_{N+1-n} &= \angle a'_{N+1-n}\end{aligned} \tag{5.75}$$

The pure real excitation constraint is applied by keeping the magnitude of excitation constant and changing the phase to 0° or 180° depending on the sign of the real part of the original excitation

$$a_n = \text{sign}(\mathcal{R}\{a'_n\})|a'_n|. \tag{5.76}$$

The dynamic range is defined as the ratio of the maximum excitation to the minimum excitation (2.25). Since a change in the largest excitation will influence the radiation pattern the most changes are made only to the smaller excitations. The phase of the excitation is preserved. If the magnitude of an excitation is below a_{off} that element is switched off.

$$a_n = \begin{cases} a'_n & \text{if } |a'_n| \geq a_{min} \\ a_{min}\dfrac{a'_n}{|a'_n|} & \text{if } a_{off} \leq |a'_n| < a_{min} \\ 0 & \text{if } |a'_n| < a_{off} \end{cases} \tag{5.77}$$

where a_{min} is the minimum allowable excitation to obtain the specified dynamic range.

The smoothness constraint is implemented by fractionally increasing the element a_n with the maximum $\frac{|a_{n\pm1}|}{|a_n|}$ until the required smoothness is obtained.

After applying the excitation constraints the power of the excitation is normalised to the total power of the original excitation:

$$\sum_{n=1}^{N} |a_n|^2 = \sum_{n=1}^{N} |a'_n|^2. \tag{5.78}$$

5.4.3 Element Patterns

Before any synthesis can be attempted the field pattern of each element, including the effects of the host vehicle on the element pattern, must be determined. Geometrical Theory of Diffraction (GTD) is an effective numerical technique for analysing the radiation of an element, taking into account the effect of the vehicle it is mounted on. Recent publications [120, 121, 113] used analytical functions for element patterns. The power patterns of the elements showed good correlation. The main difference between the analytical and GTD element patterns can be summarised as follows: Analytical element patterns do not have any phase variation (the functions are pure real), while the element patterns generated with GTD showed large phase variation off the broadside direction. The radiation pattern summation includes the field pattern and not the power pattern of the array elements. Although the power patterns of the two approaches are similar the lack of phase information in the analytical functions may cause serious inaccuracies, as will be shown later in Section 5.6.4.

Even if the radiation element used in the conformal array may have good cross polar characteristics, a slanted edge of the host vehicle will cause a cross polar component in the radiated field pattern. Thus, for the general conformal array case not only must the co-polarisation pattern be obtained, but also the cross polarisation pattern. This can also be computed using GTD. The projection method is adaptable to take both the co- and cross polarisation into account during the synthesis of conformal arrays. Geometrical Theory of Diffraction was implemented for only elliptical cylinders (of which circular arc arrays are a special case) and spherical arrays.

Cubic splines interpolation (an interpolation scheme which is continuous up to the second derivative) of the GTD element patterns of the one dimensional conformal array cases is implemented. This gives a very accurate radiation pattern even between the GTD pattern sample points. Due to a lack of computer power (CPU speed as well as memory) the two-dimensional case was programmed to use linear interpolation for both the co- and cross polarisation.

A number of analytical element patterns have also been implemented. Results of an investigation into the importance of accurate element patterns (versus analytical element patterns) are presented in Section 5.6.4.

5.5 Starting Point Selection

The choice of a particular starting point (or set of initial values) may cause any non-linear numerical optimisation algorithm to fall in a local minima, thus the initial values of the optimisation parameters (excitations in the array synthesis case) are crucial to the success of any optimisation process. A proper selection of the starting point will be close enough to the final solution to avoid falling into a trap. The choice of a good starting point should include the constraints on the excitations, for example if there is a constraint on the dynamic range of the excitations a good starting point may be obtained by a phase only synthesis where the amplitude of each element is fixed.

For uniformly spaced linear arrays the method of Orchard, Elliot and Stern [54] can be used. The method is root-based and gives a number of patterns that satisfy the pattern requirements. The one that best approximates the other constraints (eg. excitation smoothness) can be chosen. This starting point will be close to the point of convergence. For uniformly spaced planar arrays the methods of Chapter 3 or Chapter 4 will give a good initial point. However, there is no clear way to select a starting point for conformal arrays.

Finding a good starting point is not simple because of the non-linear nature of the synthesis problem. A number of different methods to obtain a good starting point is investigated in this section.

5.5.1 Radiation Pattern Mask

One obvious solution may be the excitation obtained by the back projector from the centre of the mask ($\frac{1}{2}(S_U+S_L)$) with a zero phase. The disadvantage of this approach is that a non-optimal phase distribution is forced onto the radiation pattern from the onset of the iterations; which may lead to a local minima. A possible way to overcome this difficulty is to assign some phase function or even a random phase to the mask.

5.5.2 Component Beam Technique

A number of pattern angles are chosen in the shaped beam region. For every pattern angle a pencil beam with its peak at that pattern angle is computed. We will refer to these pencil beams as *component beams*. To obtain a component beam the radiation pattern at angles in the sidelobe region is set to zero. This removes the phase ambiguity in the power synthesis problem. Maximum likelihood or weighted least squares can be used to compute the excitation of each component beam in a single step. Weighted least squares will give better sidelobe level performance as the weight of the main beam can be increased relative to the sidelobe weights. The starting radiation pattern is then the summation of each component beam, weighted with the desired value of the radiation pattern. An additional phase shift can also be applied to each of the component beams.

This is reminiscent of Woodward synthesis, except that the component beams are not orthogonal beams in general and the number of component beams used is higher than the number of orthogonal beams used in Woodward synthesis.

5.5.3 Genetic Algorithm to Obtain a Phase Function

Genetic algorithm is a powerful tool in the optimisation of non-linear functions, especially for functions of few variables. Unfortunately the large number of variables in array synthesis makes genetic algorithm unsuitable for array synthesis problems. However, by drasticly reducing the number of variables, genetic algorithm can be used to find good initial values, or warm start, for the general synthesis problem

The phase variation in the shaped beam region of an array pattern is smooth, making possible the definition of a phase function with few variables. Let us first consider shaped beams in one principal cut of the antenna pattern. The variables are a number of coordinates, each consisting of a pattern angle θ_i in the principal pattern cut and the phase α_i at that pattern angle. The pattern angle of the last coordinate is anchored at the end of the shaped beam region. The phase function $P(\theta)$ is the cubic splines interpolation between these coordinates. If I coordinates are chosen, the phase function consist of $(2I-1)$ variables.

A number of pattern angles (M) are chosen in the shaped beam region and the component beams in those directions $C_m(\theta)$ are determined as discussed in the previous section. The radiation pattern is then the summation of each component beam, weighted with the desired value of the radiation pattern as well as shifted in phase with the values of the phase function at that pattern angle θ,

$$F(\theta) = \sum_{m=1}^{M} S(\theta_m) e^{P(\theta_m)} C_m(\theta). \tag{5.79}$$

The excitation for this radiation pattern can easily be computed

$$a_n = \sum_{m=1}^{M} S(\theta_m) e^{P(\theta_m)} c_{nm} \tag{5.80}$$

where a_n is the n-th excitation and c_{nm} the n-th excitation of the of the m-th component beam.

Genetic algorithm is used to find the best values for the phase function variables. After calculating the excitation by using (5.80), the excitation constraints are applied. The cost function optimised by genetic algorithm is the total pattern error (5.71) of the radiation pattern produced by the constrainted excitation.

This calls to mind the well known Woodward synthesis method. The major differences are that the component beams are not orthogonal as well as the additional phase shift of each of the component beams.

The proposed method is as follows:

- Select a number of directions in the shaped beam region (θ_m).
- For each of these pattern directions compute a corresponding component beam $C_m(\theta)$.
- Use genetic algorithm to find the optimum phase function $P(\theta_i, \alpha_i)$.

In the case of flat-top or fan beams for both one dimensional and two dimensional arrays between 5 $(I = 3)$ and 11 $(I = 6)$ variables are needed to describe the phase function adequately.

In the case of contoured footprint patterns each phase function coordinate consists of both pattern angles (θ_i, ϕ_i) and the phase values α_i. The pattern angles are selected in a small number of rings around the direction $(0, 0)$, which is also the phase reference point. The phase function is a linear interpolation of these coordinates. Genetic algorithm optimises only the phase values α_i.

5.6 Application and Convergence

In order to get a better grasp of the convergence phenomena it is imperative to look into the algorithmic detail of the specific implementation. Two systems for selection of the pattern angles are available. The first is a fixed number of pattern angles uniformly spaced in the main beam and sidelobe regions. The second system finds all the extrema of difference between the radiation pattern and the shaping function in the main beam region; and the sidelobe peaks in the sidelobe region. All these extrema angles are incorporated into the set of pattern angles.

The algorithm is divided into an outer and an inner loop. In the outer loop the optimum absolute value for the shaping function is set (see Section 5.4.1). If the second pattern angle selection scheme is chosen a new set of pattern angles is determined as described above in each outer loop; and the radiation matrix must be recomputed. A change in either the shaping function level or the pattern angles result in a "new" synthesis problem. The inner loop uses the information forthcoming from the outer loop to perform the projection with or without relaxation. The outer loop in effect creates a new synthesis problem for the inner loop using the excitation of the previous outer loop iteration as new starting point. Convergence in the outer loop can not be guaranteed; $\xi_{k+1} \leq \xi_k$ does not hold.

If weighted least squares is used as the backward projector the inverse of the radiation matrix must be computed in each inner loop iteration; because the relative weighting (depending on the radiation pattern) changes with each iteration. This will cause a slight increase in execution time for each iteration.

Since the optimum value for the relaxation parameter (if relaxation is selected) is calculated numerically in each of the inner loops, the application of relaxation will result in a significant increase in execution time per iteration. However, relaxation should reduce the total number of iterations.

Convergence and the rate of convergence depend on a number of factors:

1. The type of backward operator: maximum likelihood method (abbreviated as "MLM") or weighted least squares (abbreviated as "WLS").
2. Whether or not relaxation is used.
3. The number and directions of far-field angles.
4. The initial or starting values.
5. Radiation pattern constraints.
6. Excitation constraints.

There exist a lot of interaction between these factors. A number of case studies have been used to gauge the performance of various options available. The first two factors will be discussed and also illustrated by case study #1; and the next two in case studies #2 and #3, respectively. The radiation pattern constraints and the excitation constraints do not influence the convergence directly, but determine some of the sets involved. Too strict constraints will result in sets with no intersection. The influence of the constraints is implicit in all case studies and examples, and will thus not be investigated on its own.

An equi-spaced linear array is used in the first three case studies because various optimal (or near optimal) synthesis methods exist for this kind of array. The first three case studies are based on a sixteen element ($N=16$), uniformly spaced linear array, with inter element spacing $d_x = 0.5\lambda$. The pattern requirement is a $\csc^2(\phi)$ main beam from

$\phi=100°$ to $\phi=140°$, with a maximum peak-to-peak ripple of 1.0dB. A sidelobe level of -20dB is required, except from 70° to the main beam where the sidelobes must be below -30dB. This is the pattern synthesised by Orchard, Elliott and Stern [54], and is often used in literature as a benchmark. The pattern obtained in [54] has a main lobe below -30dB at 90.6° and below -20dB at 142.0° ; and the dynamic range of the excitation is $DR=5.15$.

Although the choice of element patterns may not have a marked effect on the convergence, the last case study shows the importance of accurate element patterns in the analysis and synthesis of conformal arrays.

5.6.1 Case Study #1: Backward Operators and Relaxation

Two starting points will be investigated. The first set of initial values is the excitation obtained by Orchard et al. [54], with the smaller excitations increased to obtain a dynamic range of $DR=3.33$. This set of initial values is known to be close to a global minimum. The other starting point is obtained by the component beams with a genetic algorithm optimised phase distribution. The starting excitation selection will be discussed in more detail in case study #3. Both pattern angle selection systems will be used. For the selection system that include all the extrema angles, the minimum number of angles is twice the number of array elements. The number of pattern angles used in the fixed angle system is ten times the number of array elements. The trials are:

1. Orchard excitation start excitation and extrema pattern angles selection with the number of pattern angles $M \geq 32$.
2. Genetic Algorithm initial excitation and extrema pattern angles selection with the number of pattern angles $M \geq 32$.
3. Orchard excitation start excitation and fixed pattern angles with the number of pattern angles $M=161$.

In addition to the radiation pattern specifications described, the excitation is optimised to give the smallest possible dynamic range $DR=3.75$. For all the cases the inner iterations are terminated after a maximum of 50 iterations or when the error ξ_k decreased with a factor of 5.

The convergence rates for the three different trial runs are drawn in Figure 5.4. The legend used is "NM" for maximum likelihood as backward projector without relaxation; "NW" for weighted least square as backward projector without relaxation; "RM" maximum likelihood as backward projector with relaxation and "RW" for weighted least squares as backward projector with relaxation. Table 5.1 lists the execution or CPU time and number of iteration for each trial. The computer is a DEC Alpha 266 running the OFS1 Unix operating system. When comparing the convergence rates and execution times a number of conclusions can be drawn:

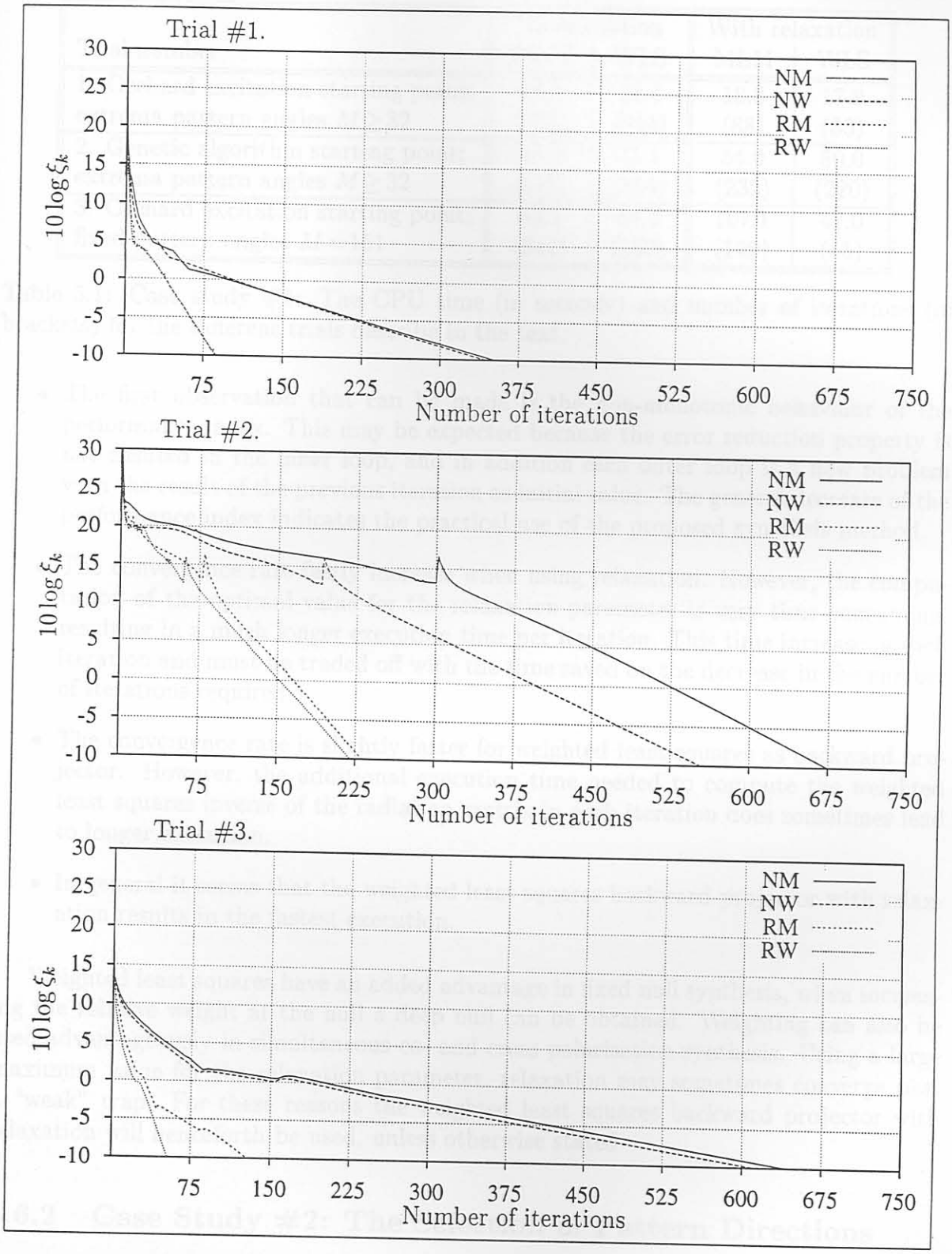

Figure 5.4: Case study #1: Convergence for the different applications. "NM" ≡ MLM without relaxation; "NW" ≡ WLS without relaxation; "RM" ≡ MLM with relaxation and "NW" ≡ WLS with relaxation.

Trial number	No relaxation MLM	No relaxation WLS	With relaxation MLM	With relaxation WLS
1. Orchard excitation starting point; extrema pattern angles $M \geq 32$	25.3 (353)	24.4 (344)	18.8 (88)	17.9 (86)
2. Genetic algorithm starting point; extrema pattern angles $M \geq 32$	50.8 (675)	41.1 (555)	54.0 (232)	50.0 (220)
3. Orchard excitation starting point; fixed pattern angles $M = 161$	63.1 (642)	63.1 (550)	107.1 (129)	47.0 (55)

Table 5.1: Case study #1: The CPU time (in seconds) and number of iterations (in brackets) for the different trials describe in the text.

- The first observation that can be made is the non-monotonic behaviour of the performance index. This may be expected because the error reduction property is not ensured in the inner loop, and in addition each outer loop is a new problem with the result of the previous iteration as initial value. The general decrease of the performance index indicates the practical use of the proposed syntehsis method.

- The convergence rate fastly increase when using relaxation. However, the computation of the optimal value for the relaxation parameter is very time consuming, resulting in a much longer execution time per iteration. This time increase in each iteration and must be traded off with the time saved on the decrease in the number of iterations required.

- The convergence rate is slightly faster for weighted least squares as backward projector. However, the additional execution time needed to compute the weighted least squares inverse of the radiation matrix in each iteration does sometimes lead to longer execution.

- In general it seems that the weighted least squares backward projector with relaxation results in the fastest execution.

Weighted least squares have an added advantage in fixed null synthesis, when increasing the relative weight at the null a deep null can be obtained. Weighting can also be used advantageously in simultaneous co- and cross polarisation synthesis. Using a large maximum value for the relaxation parameter, relaxation may sometimes converge past a "weak" trap. For these reasons the weighted least squares backward projector with relaxation will henceforth be used, unless otherwise stated.

5.6.2 Case Study #2: The Selection of Pattern Directions

The software is written such that for both pattern angles selection schemes have a higher density in the shaped beam region than the sidelobe region. No pattern angle is selected in transition regions. A number of angles are always included:

Description	M	DR	No relaxation Time	Iterations	Error	With relaxation Time	Iterations	Error
Trial 1:	*81*	*3.50*	*7.0*	*828*	*81.7*	*6.3*	*37*	*79.2*
Orchard,	161	3.50	67.9	831	25.5	31.2	58	23.7
Fixed M	241	3.50	161.3	831	8.7	132.3	58	8.1
	321	3.75	106.0	469	10.5	47.6	48	8.5

Table 5.2: Case study #2: The dynamic range, CPU time (in seconds), number of iterations and radiation pattern error for different numbers of pattern angles for the first trial.

- the start and end angles of the shaped beam region,
- the start of the sidelobe regions and
- all fixed null angles.

Four trials will be investigated using weighted least squares as backward operator with and without relaxation. The two starting points used in the previous case study will be used again. The excitation is constrainted to obtain the lowest possible dynamic range. The trials are:

1. Orchard excitation start excitation and fixed pattern angles.
2. Genetic algorithm initial excitation and fixed pattern angles.
3. Orchard excitation start excitation and extrema pattern angle selection.
4. Genetic algorithm initial excitation and extrema pattern angle selection.

Determining the fixed pattern angles is straight forward and not CPU intensive. The number of pattern angles must be large enough to ensure that all extrema angles are included in the set of angles. This would require large matrixes, resulting in long computation of the radiation matrix and its inverse. If the pattern sampling is too coarse not every peak outside pattern mask will be included in numerical error function, and thus may not be representative of the true error. With the extrema angle selection scheme the numerical search algorithm is used to obtain the pattern extrema in the outer loop. This operation is very CPU intensive. Since the number of extrema is in the same order as the number of array elements, the matrixes are smaller and less time is spent on their computation.

The results from the different trials are tabulated in Table 5.2 and Table 5.3. The different trials have very similar results in the radiation pattern as well as the excitation, as can be seen in Figure 5.5. In this figure the radiation pattern and excitation of the emphasised rows in Tables 5.2 and 5.3 are shown.

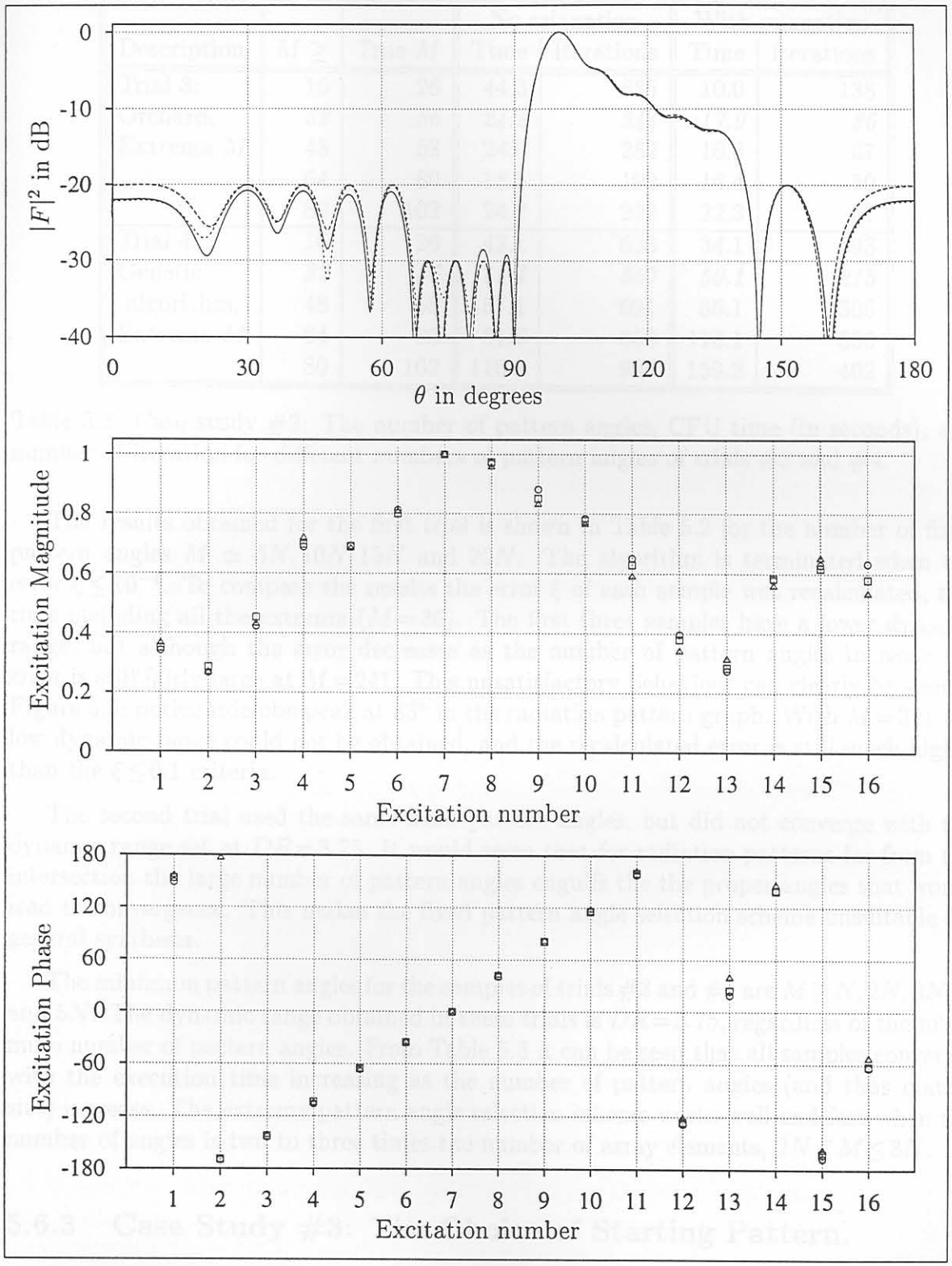

Figure 5.5: Case Study #2: The radiation pattern (top) and excitation amplitude (middle) and phase (bottom) for some trials (see text). (Legend: $\square \equiv$ first trial, $\odot \equiv$ third trial and $\triangle \equiv$ fourth trial.)

Description	$M \geq$	True M	No relaxation Time	No relaxation Iterations	With relaxation Time	With relaxation Iterations
Trial 3:	16	26	44.3	885	10.0	138
Orchard,	*32*	*36*	*24.2*	*344*	*17.9*	*86*
Extrema M	48	58	24.0	282	18.3	67
	64	80	18.5	192	16.4	50
	80	102	24.2	222	22.3	57
Trial 4:	16	26	42.1	633	34.1	193
Genetic	*32*	*36*	*41.1*	*557*	*50.1*	*215*
algorithm,	48	58	57.1	691	86.1	306
Extrema M	64	80	81.6	856	118.1	350
	80	102	116.1	998	159.2	402

Table 5.3: Case study #2: The number of pattern angles, CPU time (in seconds), and number of iteration for different numbers of pattern angles of trials #3 and #4.

The results obtained for the first trial is shown in Table 5.2 for the number of fixed pattern angles $M \simeq 5N, 10N, 15N$ and $20N$. The algorithm is terminated when the error $\xi \leq 10^{-4}$. To compare the results the error ξ of each sample was recalculated, this time including all the extrema ($M = 36$). The first three samples have a lower dynamic range, but although the error decreases as the number of pattern angles increase the error is still fairly large at $M = 241$. This unsatisfactory behaviour can clearly be seen in Figure 5.5; notice sidelobe peak at 83° in the radiation pattern graph. With $M = 321$ the low dynamic range could not be obtained, and the recalculated error is still much higher than the $\xi \leq 0.1$ criteria.

The second trial used the same fixed pattern angles, but did not converge with the dynamic range set at $DR = 3.75$. It would seem that for radiation patterns far from the intersection the large number of pattern angles engulfs the the proper angles that would lead to convergence. This makes the fixed pattern angle selection scheme unsuitable for general synthesis.

The minimum pattern angles for the samples of trials #3 and #4 are $M \geq N, 2N, 3N, 4N$ and $5N$. The dynamic range obtained in these trials is $DR = 3.75$, regardless of the minimum number of pattern angles. From Table 5.3 it can be seen that all samples converge, with the execution time increasing as the number of pattern angles (and thus matrix size) increase. The extrema pattern angle selection scheme works well and fast when the number of angles is two to three times the number of array elements, $2N \leq M \leq 3N$.

5.6.3 Case Study #3: The Choice of Starting Pattern.

The purpose of this case study is to illustrate the importance of a good starting point, as well as to show the relative performance of the different starting pattern selection algorithms. For each starting values the dynamic range of the excitation is interactively

Starting pattern selection	Dynamic Range
Orchard, Elliot and Stern's synthesis method	3.75
Unit excitation distribution	4.15
Pattern mask with zero phase distribution	4.90
Pattern mask with random phase distribution	4.55
Component beams with zero phase distribution	3.90
Component beams with linear phase distribution	3.90
Component beams with random phase distribution	4.95
Component beams with Genetic algorithm, 7 parameters	4.00
Component beams with Genetic algorithm, 9 parameters	3.75
Component beams with Genetic algorithm, 11 parameters	3.90

Table 5.4: Case study #3: The dynamic range obtained by the various starting pattern selection schemes

lowered to obtain a suitable radiation pattern with the excitation with the lowest dynamic range. Weighted least squares is selected as the backward projector and relaxation is used.

In the case of pencil beams a single component beam will be a good starting pattern. However, in the case of shaped or contoured beams a good representation of the phase in the shaped region is very important as the phase distribution tends to carry over from iteration to iteration. This phenomenon has also been noted by others [141].

To illustrate the component beam approach, the top graph in Figure 5.6 shows some possible component beams for this case. The bottom graph displays the component beam starting pattern with the phase function optimised by genetic algorithm with nine parameters, as well as the final pattern obtained with the synthesis method. The radiation pattern obtained with Orchard's synthesis method is also drawn as a reference.

The best dynamic range obtained for each initial values selection method is tabulated in Table 5.4. From the different dynamic range values it is clear that a multitude of traps do exist. As expected starting points that do not consider the phase distribution in the shaped beam region do fall into traps. The genetic algorithm must optimise few enough variables to obtain an answer in a reasonable time. However, too few parameters will result in a function that does not adequately describe the phase distribution. With this in mind, the table shows that nine parameters are a good choice for the shaped beam synthesis problem in the case study. An increase in the shaped beam beamwidth or, to a lesser extent, an increase in the number of elements will require more variables. A "simpler" beam shape, like a flat-top beam, less variables will be adequate.

It does not seem unreasonable to assume that the Orchard synthesis method result in an excitation very close to the optimum. Since the excitation obtained with the nine parameter component beam starting pattern result in almost exactly the same excitation (less than 0.3% difference in magnitude and less than 0.2° difference in phase) one may assume that the component beam approach with genetic algorithm to optimise the phase distribution will result in near optimum patterns. This, of course, cannot be guaranteed.

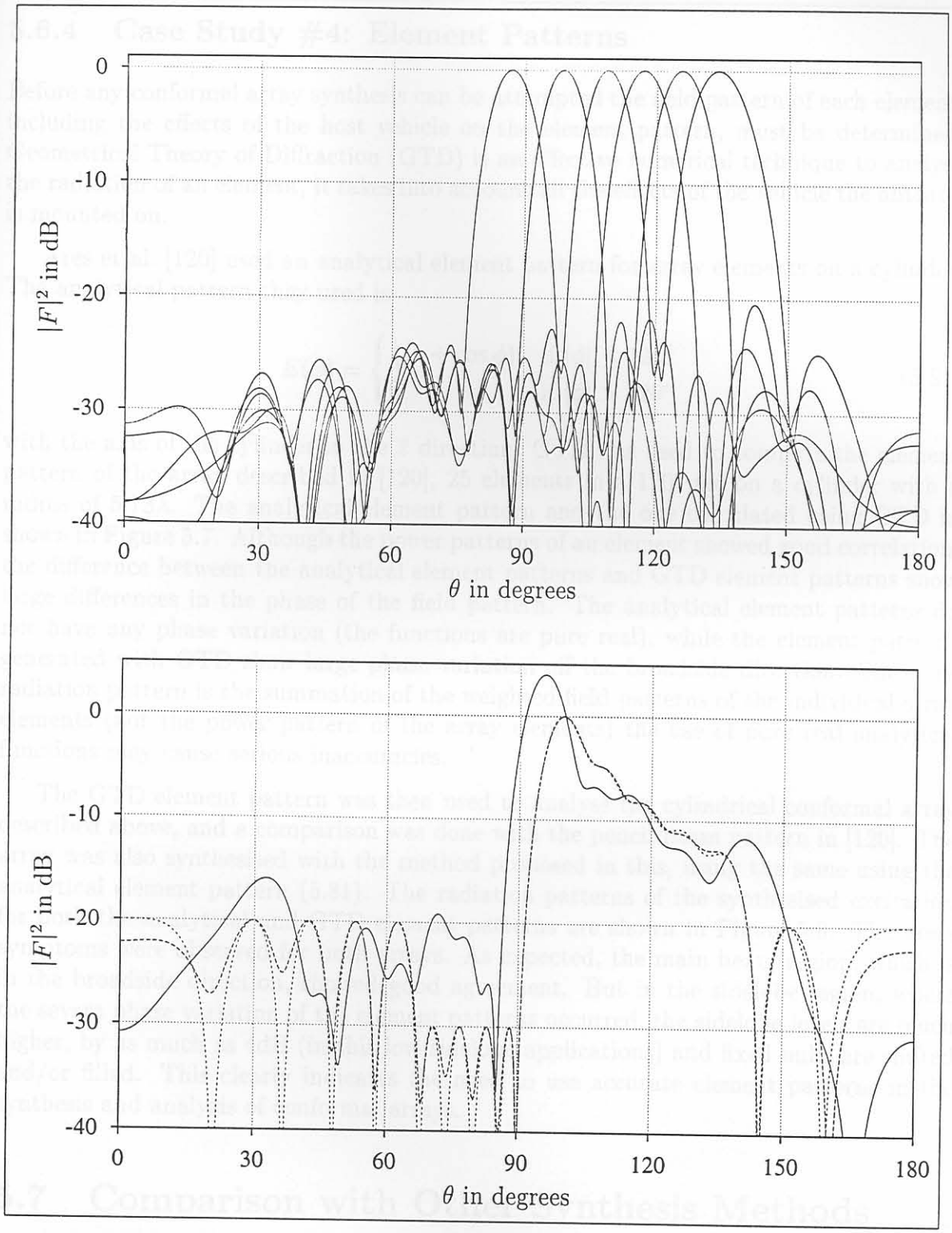

Figure 5.6: Case study #3: The top graph display the component beams used to obtain the starting pattern. The starting pattern shown as the solid trace in the bottom graph. The dashed line in the bottom graph represent the final optimised pattern and the dotted line pattern obtained by Orchard's method (as a reference pattern).

5.6.4 Case Study #4: Element Patterns

Before any conformal array synthesis can be attempted the field pattern of each element, including the effects of the host vehicle on the element pattern, must be determined. Geometrical Theory of Diffraction (GTD) is an effective numerical technique to analyse the radiation of an element, it takes into account all the effects of the vehicle the antenna is mounted on.

Ares et al. [120] used an analytical element pattern for array elements on a cylinder. The analytical pattern they used is

$$E(\phi) = \begin{cases} \frac{1}{3}(1+\cos\phi) & \text{if } |\phi| \leq 120^\circ \\ 0 & \text{if } |\phi| > 120^\circ \end{cases} \tag{5.81}$$

with the axis of the cylinder in the $\hat{z}$ direction. GTD was used to compute the element pattern of the array described in [120]; 25 elements in a 120° arc on a cylinder with a radius of 5.73λ. The analytical element pattern and the one calculated using GTD in shown in Figure 5.7. Although the power patterns of an element showed good correlation, the difference between the analytical element patterns and GTD element patterns show large differences in the phase of the field pattern. The analytical element patterns do not have any phase variation (the functions are pure real), while the element patterns generated with GTD show large phase variation off the broadside direction. Since the radiation pattern is the summation of the weighted field patterns of the individual array elements (not the power pattern of the array elements) the use of pure real analytical functions may cause serious inaccuracies.

The GTD element pattern was then used to analyse the cylindrical conformal array described above, and a comparison was done with the pencil beam pattern in [120]. The array was also synthesised with the method proposed in this, using the same using the analytical element pattern (5.81). The radiation patterns of the synthesised excitation for both the analytical and GTD element patterns are shown in Figure 5.8. The same symptoms were observed for both arrays. As expected, the main beam region, which is in the broadside direction, showed good agreement. But in the sidelobe region, where the severe phase variation of the element patterns occurred, the sidelobe levels are much higher, by as much as 4dB (in this low sidelobe applications) and fixed nulls are shifted and/or filled. This clearly indicates the need to use accurate element patterns in the synthesis and analysis of conformal arrays.

5.7 Comparison with Other Synthesis Methods

5.7.1 Iterative Least Squares Methods

Carlson and Willner [141] first suggested using weighted least squares in the synthesis of arrays. The weighted least squares is analytical and yields an optimal pattern, for the

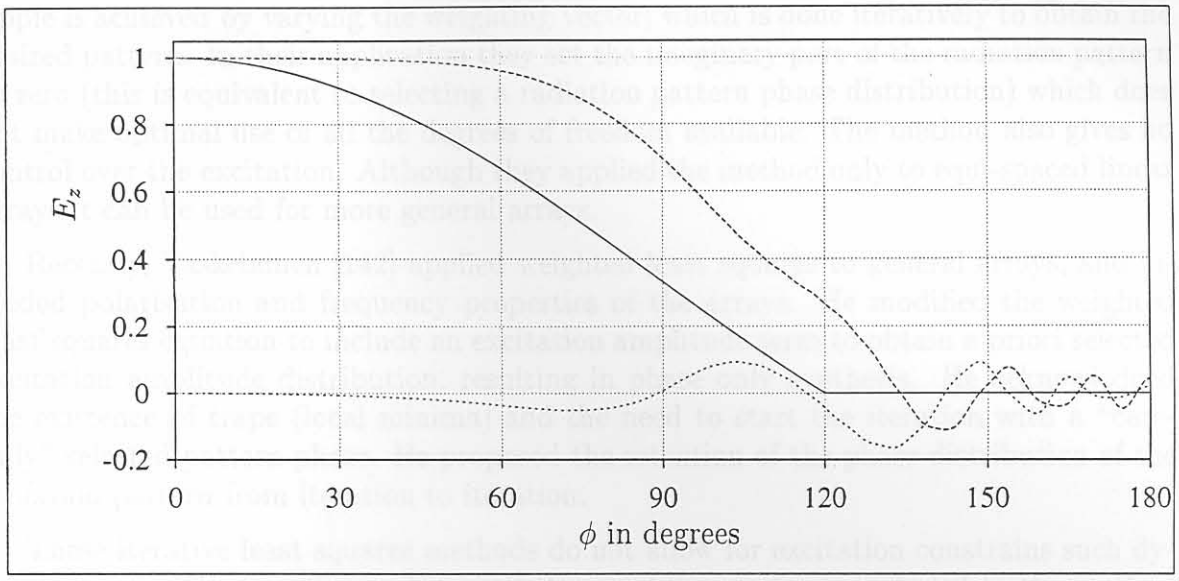

Figure 5.7: Case study #4: The analytical element pattern (the solid line) and the real (dashed line) and imaginary (dotted line) parts of the GTD element pattern.

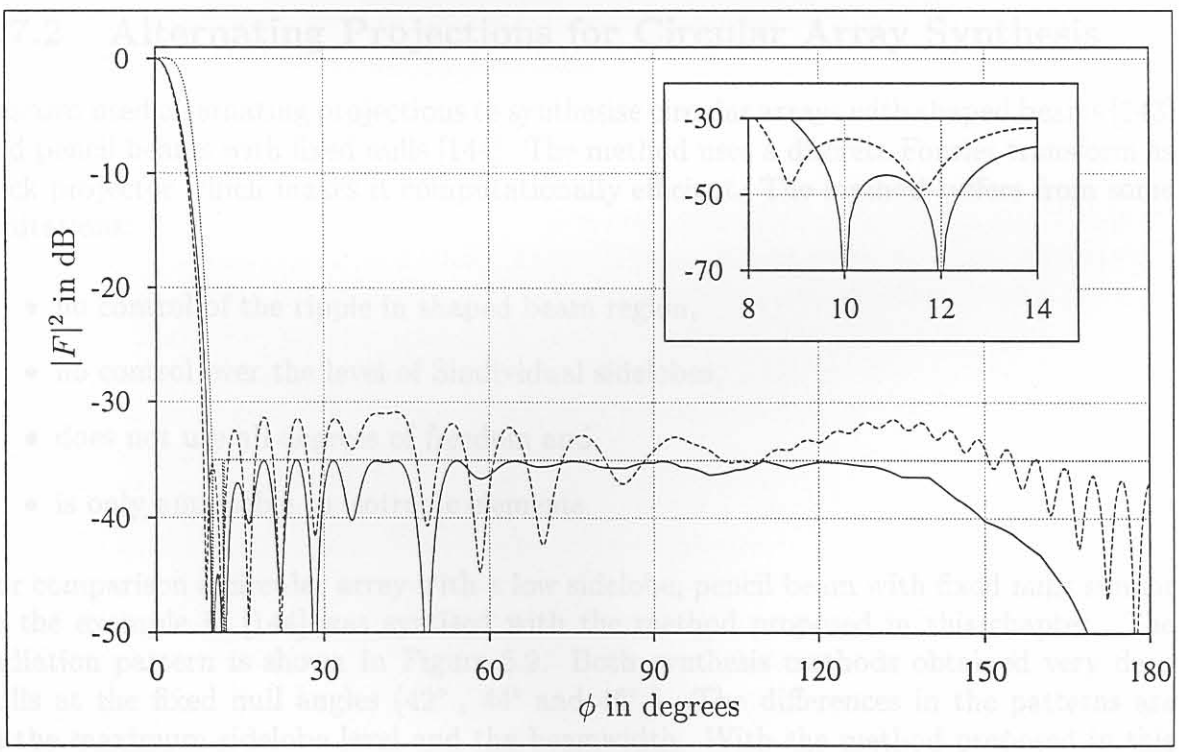

Figure 5.8: Case study #4: The solid curve is synthesised radiation pattern with analytical element patterns; the dashed curve is same excitation but with GTD element patterns. The magnification shows the region of the radiation pattern at the fixed null positions.

specific set of values, in a single computation. Control of the sidelobe level or main beam ripple is achieved by varying the weighting vector; which is done iteratively to obtain the desired pattern. In their application they set the imaginary part of the radiation pattern to zero (this is equivalent to selecting a radiation pattern phase distribution) which does not make optimal use of all the degrees of freedom available. The method also gives no control over the excitation. Although they applied the method only to equi-spaced linear arrays it can be used for more general arrays.

Recently, Vaskelainen [142] applied weighted least squares to general arrays, and included polarisation and frequency properties of the arrays. He modified the weighted least squares equation to include an excitation amplitude term to obtain a priori selected excitation amplitude distribution, resulting in phase only synthesis. He acknowledged the existence of traps (local minima) and the need to start the iteration with a "carefully" selected pattern phase. He proposed the retention of the phase distribution of the radiation pattern from iteration to iteration.

These iterative least squares methods do not allow for excitation constrains such dynamic range. The iterative variation of the weighting vector is included in the method proposed in the thesis when the weighed least squares is used as the backward operator (5.72).

5.7.2 Alternating Projections for Circular Array Synthesis

Vescovo used alternating projections to synthesise circular arrays with shaped beams [143] and pencil beams with fixed nulls [144]. The method uses a discrete Fourier transform as back projector which makes it computationally efficient. The method suffers from some limitations:

- no control of the ripple in shaped beam region,
- no control over the level of Sindividual sidelobes,
- does not use all degrees of freedom and
- is only applicable to isotropic elements.

For comparison a circular array with a low sidelobe, pencil beam with fixed nulls similar to the example in [144] was syntised with the method proposed in this chapter. The radiation pattern is shown in Figure 5.9. Both synthesis methods obtained very deep nulls at the fixed null angles (42° , 44° and 46°). The differences in the patterns are in the maximum sidelobe level and the beamwidth. With the method proposed in this chapter a uniform sidelobe level of -52dB was obtained (compared to a maximum sidelobe level of -37dB) with an additional null between the main lobe and the fixed nulls.

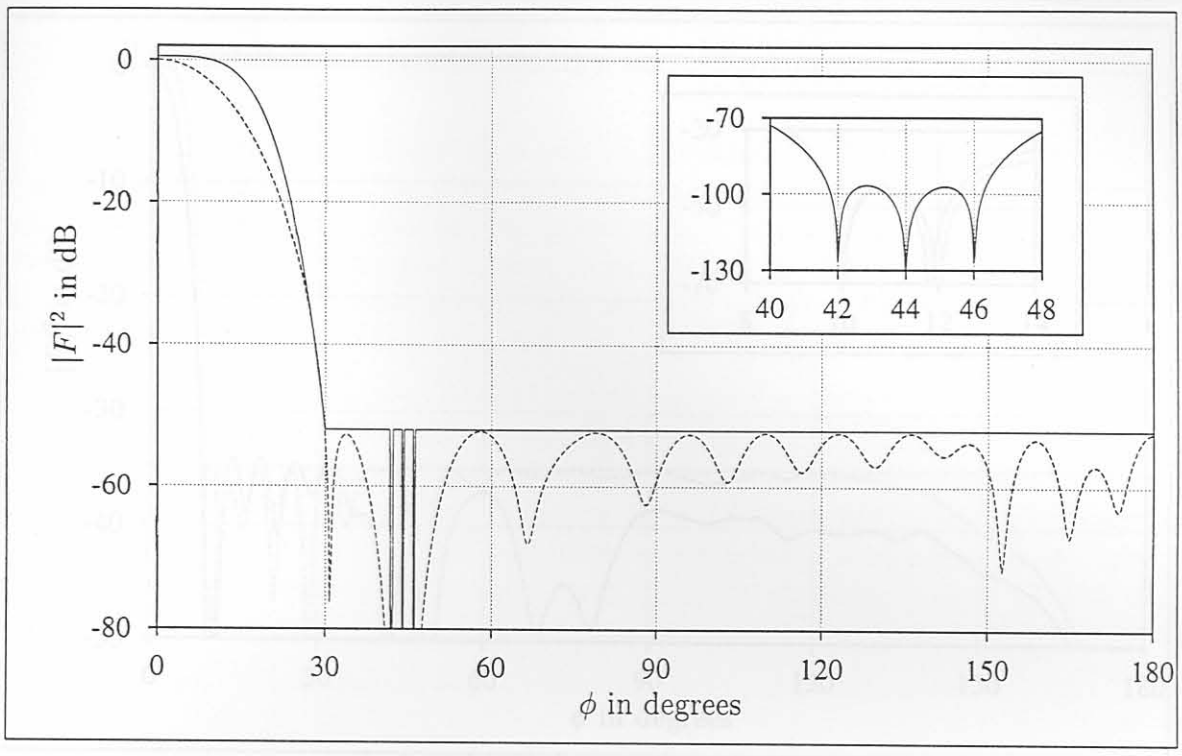

Figure 5.9: Radiation pattern for circular array, the magnification shows the radiation pattern at the fixed nulls

5.7.3 Generalised Projection Method

Recently Bucci, D'Elia and Romito extended the generalised projection method to power synthesis for conformal arrays [113]. They mention the problem of traps, and in order to avoid being trapped in local minima they adopted a non-standard choice of output variables; the power pattern instead of the field values. The backward operator can be performed by any minimisation algorithm. They used a self-scaled version of the BFGS (Broyden-Fleatcher-Golfarb-Shanno) method which takes into account the quadratic nature of the radiation pattern to be optimised.

They applied the method to synthesise contoured footprint and fan beam patterns for both a rectangular planar array and cylindrical array. The radiation patterns they published in [113] have high sidelobes in the principal planes, with very low sidelobes in the off principal plane cuts. This indicates a non-optimal solution to the synthesis problem. Sidelobes in rings around the main beam, as those in example 5.8.4 (rectangular array, see Figure 5.15) and example 5.8.5 (conformal array, see Figure 5.17), indicate a better solution.

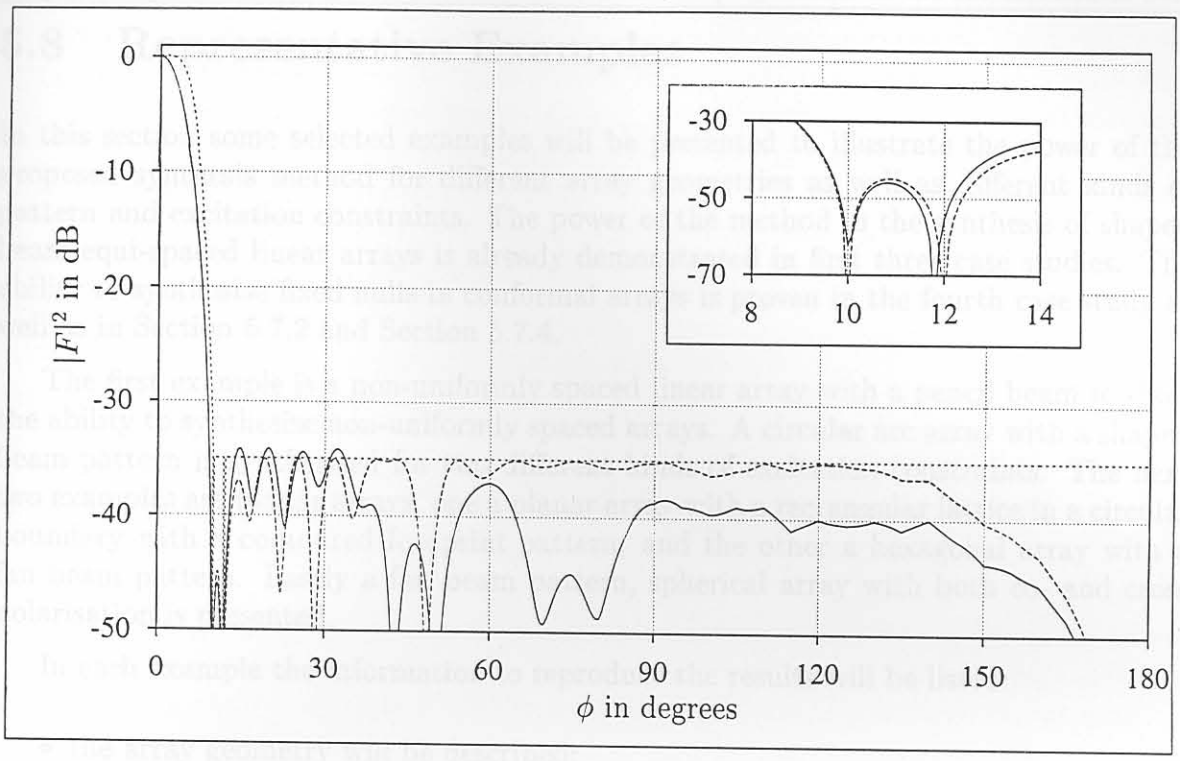

Figure 5.10: The radiation patterns obtained with simulated annealing (solid curve) and from the intersection of sets method (dashed curve). The magnification shows the region of the radiation pattern at the fixed nulls.

5.7.4 Simulated Annealing

Ares et al. [120, 121] used simulated annealing to synthesise conformal arrays. The cost function, the function to be minimised, can include terms to control the radiation pattern as well as terms placing constraints on the excitation. The authors claim that simulated annealing avoids local minima and converges to the global minimum of the cost function. To refute this claim one only has to obtain better results in one case.

Ares et al. [120] investigated a 25 element, 120° circular arc array on a cylinder with a radius of 5.73λ. The object of their first example is to synthesise a pencil beam with their fixed nulls at $\pm 10°$ and $\pm 12°$, while minimising the dynamic range. The authors did not meet the sidelobe level specification of -35dB they set, four sidelobe peaks are above this level with the highest peak at -34.2dB. The dynamic range they achieved is $DR=6.17$. For comparison, the dynamic range was iteratively minimised with the intersection of sets approach, while maintaining the same pattern requirements The same analytical element patterns were used. The dynamic range improved from $DR=6.17$ to $DR=4.85$, in addition the sidelobe level specification of -35dB was achieved. Thus a minima closer to global minimum was obtained with the method proposed in this chapter compared to the results obtained with simulated annealing. Both radiation pattern are shown in Figure 5.10, due to the symmetrical pattern only one half is shown.